



Microstructure Evolution and Shear Strength Study of Sn–9Zn and Sn–8Zn–3Bi on Cu Substrate

Ramani Mayappan¹ · Zainal Arifin Ahmad²

Received: 16 July 2023 / Revised: 24 September 2023 / Accepted: 2 October 2023 / Published online: 17 October 2023
© The Korean Institute of Electrical and Electronic Material Engineers 2023

Abstract

In electronics assembly, solder joints not only serve as mechanical supporters-, but also as heat removers. Therefore, solder joint reliability is a major concern not only during production, but also during the life time of electronic products. It can be pointed out that reliability of solder joint determines the lifetime of electronics products. This issue becomes more important with the use of Pb-free soldering alloys. This study focuses on the reliability of Sn–9Zn and Sn–8Zn–3Bi lead-free solder joints with Cu substrates. This study deals with interface intermetallic morphology, solder joint strength and fracture surface analysis after isothermal aging at 50, 100, and 150 °C for 100, 250, and 500 h. For all aging conditions, a flat Cu₅Zn₈ intermetallic was formed, and as the aging conditions increased, Cu atoms diffused through the intermetallic to form isolated Cu₅Zn₈ intermetallics in the bulk solder. Furthermore, Sn atoms from bulk the solder diffused through the intermetallic to form Cu₆Sn₅ on the Cu side. The formation of a thick Cu₅Zn₈ intermetallic and the diffusion of Sn and Zn atoms created a depletion zone near the solder/intermetallic boundary, which weakened the joint strength. As the intermetallic layer thickness increased, the joint strength decreased as the aging increased. The fracture path generally occurred at the bulk solder/intermetallic boundary under all aging conditions.

Keywords Intermetallic · Fracture surface · Sn–Zn–Bi solder · Shear strength · Reliability · Pb-free solder

1 Introduction

Tin–Lead solder has been one of the main components in the electronic manufacturing industry for years because of its low melting temperature, good wetting, good ductility, and long shelf life. However, Lead, is the most dangerous heavy metal affecting the health and environment. So, due to its toxicity, legislation and regulations have been put in place to prohibit its use, which presents a significant challenge to conventional electronic assembly technology.

In recent years, there has been a rising push to replace lead-based solder alloys with lead-free alternatives. Hence, the evolution of electronic products has made “lead-free” a

trend and researchers are working to find alternative lead-free packaging solders to replace the conventional Sn–Pb solder.

Over the years, many tin-rich lead-free solders have been proposed, some of which are already in commercial use to replace Pb-containing solders. Solder joints in electronic products provide electrical continuity and thermal dispersion, and experience mechanical stress during their life-time [26]. Because the mechanical behavior of lead-free solder joints is a major issue in electronic industries, knowledge of the stress/strain properties of solder joints under extreme conditions is required.

With the introduction of newer and smaller portable devices, the robustness of the product is more important when dealing with the mechanical properties and intermetallic formation in solder joints. With smaller devices, the size of solder joints decreases (high density) and speed [1, 2, 6, 27]. A smaller solder size means that the ratio between the intermetallic phase and solder volume increases. This intermetallic ratio increment results in dominant mechanical properties because solder and intermetallic have different thermal expansion coefficients [3, 11]. Choudhury and Ladani [4] point out that with

✉ Ramani Mayappan
ramani@uitm.edu.my

¹ Faculty of Applied Sciences, Universiti Teknologi MARA, Cawangan Perlis, Kampus Arau, 02600 Arau, Perlis, Malaysia

² School of Materials and Minerals Resources Engineering, Engineering Campus, Universiti Sains Malaysia, 14300 Nibong Tebal, Pulau Pinang, Malaysia

higher intermetallic volume, shear behavior and failure mechanisms may change drastically. During usage and in the presence of heat, the intermetallic compound becomes thicker and unstable owing to its brittleness. This leads to crack formation and solder joint failure [5, 10, 12, 22, 25]. Hence, intermetallic compounds play an important role in electronic packaging [9].

Although there are many available lead-free solders, Sn–9Zn and Sn–8Zn–3Bi solders are still potential replacements for Sn–Pb solder. These two solders behave differently compared to Sn–Pb or Sn–Ag–Cu solders when Cu is used as the metallization finish. Both solders with a Cu substrate will form Cu–Zn intermetallics at the interface instead of Cu–Sn intermetallics. During the initial soldering, an intermediate thin Cu–Zn₅ layer formed near the solder and a flat Cu₅Zn₈ intermetallic formed near the Cu substrate [24]. However, as soldering or aging temperature/time increases, the Cu–Zn₅ intermetallic transforms to Cu₅Zn₈ [14, 16]. Although Cu₅Zn₈ is the dominant intermetallic formed, in the later stage of aging, island-type Cu₆Sn₅ will start to form, which will significantly affect the reliability of solder joint [16].

The addition of Bi to lead-free solders has some advantages. In Sn–Ag–Cu (SAC) solders, the addition of Bi improves its solder joint shear strength [15, 23] and drop impact performance [21]. This improvement due to solid-solution strengthening of β -phase Sn and/or precipitation strengthening of the Bi phase [19, 28, 29]. Hu et al. [7] reported that the addition of Bi to SAC solder, increased its hardness from 0.095 to 0.141 GPa when the Bi content increased from 1 to 3 wt%.

The presence of Bi in the Sn–8Zn–3Bi solder refines its microstructure [17] and improves its wetting force and contact angle [18] on a copper substrate. Furthermore, Bi retarded the Cu₅Zn₈ intermetallic growth and increases the activation energy from 44.05 to 55.36 kJ/mol for Sn–9Zn and Sn–8Zn–3Bi, respectively [16].

Because the intermetallic thickness and solder microstructure change in the presence of heat, it can be concluded that thermal aging significantly affects the solder joint strength. Therefore, the joint strength performance after aging is an important tool for evaluating the bonding strength over the shelf life of electronic products.

Sn–9Zn and Sn–8Zn–3Bi were investigated as potential lead-free solder candidates using the single-lap shear technique. They were reacted on a copper substrate and aged at different temperatures for different durations. The intermetallic morphology, thickness, joint strength, and fracture morphology were compared.

2 Experimental

Table 1 shows the X-ray fluorescent (XRF) analyses of the Sn–9Zn and Sn–8Zn–3Bi solders used in this study. The analysis shows the weight (%) of 90.6Sn–9.1Zn and 89Sn–8.3Zn–3.0Bi for the 91Sn–9Zn and 89Sn–8Zn–3Bi solders, respectively. Although a small amount of Pb was present in the Sn–9Zn and Sn–8Zn–3Bi solders, it still complies with the RoHS Directive, which limits the maximum of 0.1 wt% Pb in solders.

An aluminium plate was placed on the hot plate. The Cu-solder-Cu joint was soldered manually onto the plate. The temperature profile that the solder undergoes during soldering is plotted with respect to time in Fig. 1. The temperature was measured using two thermocouples (each one on a hot plate and aluminium plate) connected to a multi-functional digital meter model UNI-T. Temperature was increased at a rate of approximately 30 °C/min. Upon reaching 220 °C, the hot plate was switched off and left to cool. The temperature was increased to a maximum of (250 ± 5) °C before decreasing at a cooling rate of approximately 10 °C/min. These procedures enable the temperature to be maintained above 200 °C for approximately 4.5 min. It is important to maintain the solders in their liquid state for the duration of time for interactions to occur.

A 1.5 mm thickness dog-bone Cu was cut in the middle to form two parts. 0.2 g the solder alloy was sandwiched between the two Cu ends. To obtain the desired solder joint area and gap thickness, Cu substrates were placed

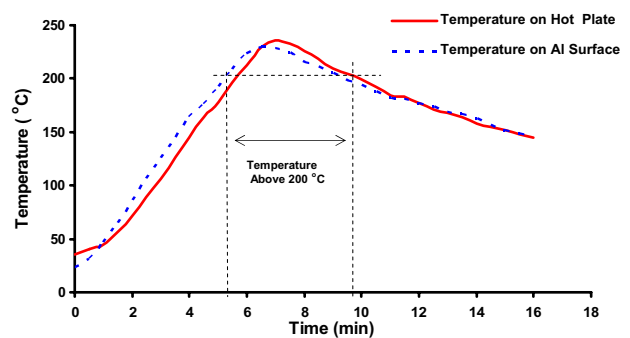


Fig. 1 Soldering temperature profiles on hotplate and aluminium plate

Table 1 Elemental compositions of solders

Solder	Weight (%)						
	Sn	Zn	Pb	Bi	Fe	Ni	Cu
Sn–9Zn	90.58	9.10	0.09	0.01	0.09	0.02	0.11
Sn–8Zn–3Bi	88.50	8.29	0.08	2.96	0.07	0.02	0.08

in a setup, as shown in Fig. 2. This setup limits the solder joint spread area to $(4 \times 8) \text{ mm}^2$ and 0.5 mm in thickness.

The zinc chloride flux was used in this study. Soldering was performed based on the temperature profiles shown in Fig. 1. Optical images of the Cu/solder/Cu joints are shown in Fig. 3.

Because temperature and storage time influence intermetallic growth, and bonding strength, soldered samples were placed in an oven at various temperatures. The joints were aged at 50, 100, and 150 °C for 100, 250, and 500 h, respectively. Longer aging times were not selected because of the brittleness of solder joints. For each aging condition, six samples were tested, with one sample allocated for the intermetallic study. For the intermetallic study, the solder joint was cross-sectioned and mounted using an epoxy resin. The solder joint was polished to smooth the surface before being analyzed with FESEM operating in the backscatter mode, and energy dispersive X-ray (EDX) was used to determine the elemental compositions. Based on the elemental composition and phase diagram, the phases presence was determined. The thickness of the intermetallic formed at the interface was measured by using Image-J software. The thickness was measured by dividing the total area of the intermetallic layer by the length of the FESEM micrograph.

The lap area $(8 \times 4) \text{ mm}^2$ and initial length ($l_0 = 4 \text{ mm}$) were used as input data for the stress and strain calculations, respectively. The load was applied parallel to the solder joint layer with a crosshead speed of 0.2 mm/min and the test was performed at room temperature. The ductility of the solder joint was measured from the strain at failure. The values of maximum stress and strain at failure are shown in Fig. 4. Specimens after tensile test were examined under FESEM to observe the fracture mode.

3 Results and Discussion

3.1 Intermetallic Formation

The relationships between intermetallic formation, strain at failure of solder joints and shear strength were investigated and discussed. Figure 5 shows the soldered solder joints for Sn–9Zn and Sn–8Zn–3Bi lead-free solders. Both display two

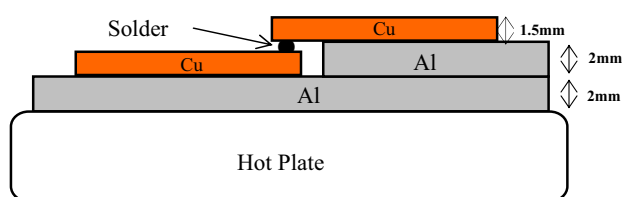


Fig. 2 Shear joint set up

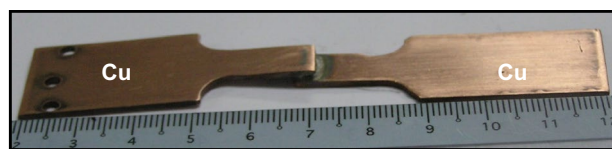


Fig. 3 Single lap dog-bone shape for Cu/solder/Cu joints (measurements in mm)

intermetallic layers: layer 1, a scallop type, and layer 2, a continuous morphology.

Further details of aging are shown in Fig. 6. EDX analysis (spot 1) confirmed that layer 1 was next to the solder as a Cu–Zn₅ intermetallic with some Sn dissolved in it. Layer 2, near the Cu substrate (spot 2), had a ratio of 48Cu–52Zn by wt%. Based on these ratios, the intermetallic compound was concluded to be Cu₅Zn₈. The EDX elemental compositions of the samples are presented in Table 2.

As aging progressed, Sn from the bulk solder diffused towards the Cu substrate by penetrating the intermetallic layer (spot 3). Cu and Zn were also detected at this spot. Cu is from the substrate diffusing towards the bulk solder. These Sn reacted with Cu to form an isolated intermetallic phase on the Cu side, as shown in Fig. 6b. This phase is in grey contrast with that of 39Cu–55Sn–6Zn (in wt%) composition (spot 4). This phase was identified as the Cu₆Sn₅ phase, and similar findings have been reported elsewhere [16, 22]. Diffusion of Sn with some Bi was also observed in the Sn–8Zn–3Bi solder, as indicated by EDX at spot 5 (Fig. 7a).

Spot 6 shows the Cu₅Zn₈ intermetallic formation in the Sn–8Zn–3Bi/Cu system with a ratio 41Cu–49Zn–6Sn–40. Although no Sn-rich spots were observed for the Sn–8Zn–3Bi/Cu system at this temperature, some Sn was detected using EDX. The diffusion of Sn atoms through the Cu₅Zn₈ intermetallic was delayed, which may have been due to the presence of Bi in the solder.

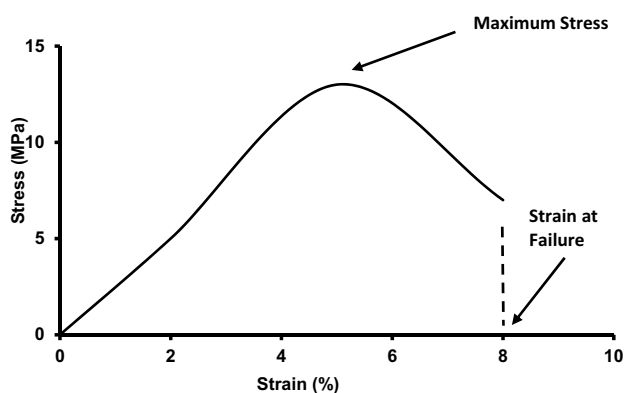


Fig. 4 Example of stress–strain curve

Fig. 5 FESEM micrograph for as-soldered **a** Sn–9Zn/Cu **b** Sn–8Zn–3Bi/Cu joint

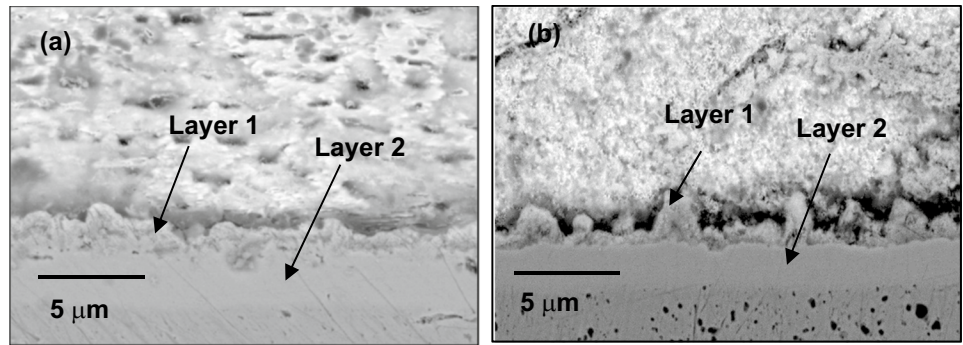


Fig. 6 FESEM micrograph for Sn–9Zn/Cu joint aged at **a** 100 °C for 500 h, **b** aged at 150 °C for 500 h

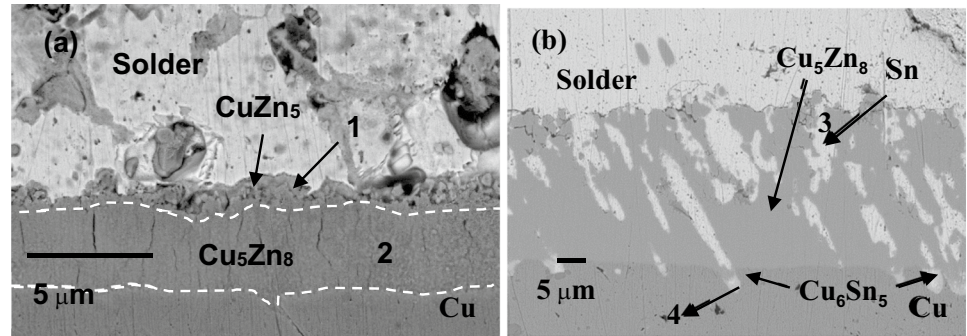


Table 2 EDX elemental analysis

Spot	Wt%						Compound/element
	Sn	Cu	Zn	O	C	Bi	
1	15.68	35.87	48.45	–	–	–	CuZn ₅
2	–	48.48	51.52	–	–	–	Cu ₅ Zn ₈
3	80.71	5.58	6.31	5.24	2.15	–	Sn with some other elements dissolved
4	54.57	39.42	6.00	–	–	–	Cu ₆ Sn ₅ with some Zn dissolved
5	87.78	4.01	5.78	–	–	2.42	Sn with some other elements dissolved
6	5.88	41.49	48.60	3.93	–	–	Cu ₅ Zn ₈
7	87.86	4.22	4.22	–	–	4.41	Sn with some other elements dissolved
8	–	–	2.50	3.96	–	93.54	Bi
9	78.98	–	1.92	4.10	12.20	2.80	Sn with some other elements dissolved

Fig. 7 FESEM micrograph for Sn–8Zn–3Bi/Cu joint aged at 150 °C for **a** 100 and **b** 500 h

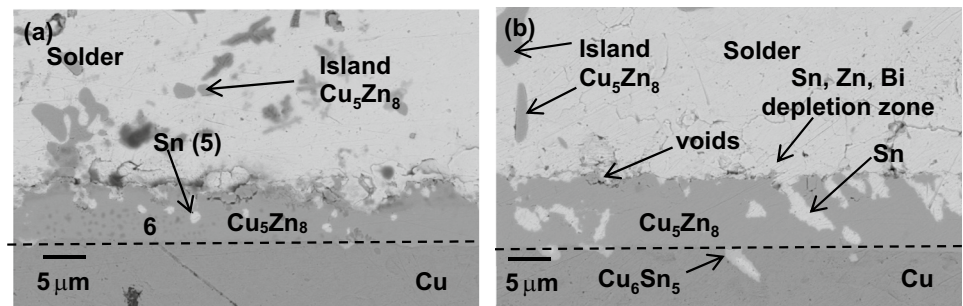


Figure 7b shows the aging of the Sn–8Zn–3Bi/Cu joint at 150 °C for 500 h. Sn diffuses (with some Bi and Zn) from the solder towards the Cu substrate and reacts with Cu to form an island Cu₆Sn₅ intermetallic. The formation

of voids/cracks at the boundary may be attributed to differences in the thermal expansion between the intermetallic phase and solder. Furthermore, some Cu atoms diffused through the intermetallic layer and moved towards the bulk

solder-forming island-type Cu_5Zn_8 . The diffusion of Sn and Zn atoms created a depletion zone at the boundary.

A magnified image of the Sn–8Zn–3Bi/Cu joint aged at 150 °C for 500 h is shown in Fig. 8. Massive diffusion of Sn towards the Cu substrate and the formation of voids near the IMC/solder interface can be clearly seen. EDX analysis showed that some Bi dissolved in Sn (spot 7). The Sn–8Zn–3Bi solder microstructure after aging at 50 °C for 500 h is shown in Fig. 8b. The Sn–8Zn–3Bi bulk solder displayed a Zn groove with some Bi precipitates in the Sn matrix (spot 8). The precipitation of Bi is due to its solubility in Sn of less than 1 wt% as reported by Zhao et al. [30].

The FESEM image of the Cu/solder/Cu solder joint at smaller magnifications is shown in Fig. 9. The movement of the Sn atoms towards the Cu substrate is clearly shown. Both Sn–9Zn and Sn–8Zn–3Bi exhibited eutectic systems. The Zn phase is homogeneously dispersed in the β -Sn matrix.

The intermetallic layer thickness measured at the interface is shown in Fig. 10. The addition of Bi clearly retarded the growth of the Cu_5Zn_8 intermetallic compound. However, Bi coarsening was not observed near or at the interface. A similar observation was reported by Nishikawa et al. [20] for Sn–Bi solder joints. Detailed descriptions of intermetallic formation and growth rate have been discussed elsewhere [16].

3.2 Aging Temperature and Time Effect on Shear Strength

Figures 11 and 12 show the strain at failure and the shear strength of the Cu/Sn9Zn/Cu and Cu/Sn8Zn3Bi/Cu joints, respectively. The strain at failure indicates the maximum change in the length before the solder joint breaks. Aging at 50 °C did not significantly change the strain at failure for

Fig. 8 **a** Higher magnification (2000X) FESEM micrograph for Sn–8Zn–3Bi/Cu joint aged at 150 °C for 500 h, **b** Solder microstructure of Sn–8Zn–3Bi solder aged at 50 °C for 500 h

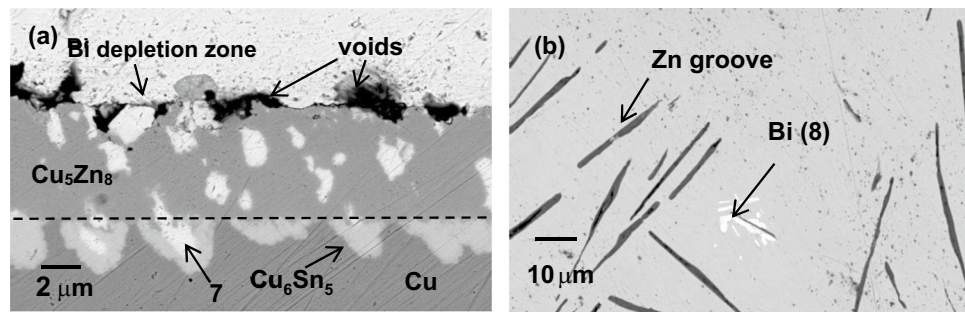


Fig. 9 Cu/solder/Cu interface for **a** Sn–9Zn (Magnification 100 \times) aged at 150 °C for 500 h and **b** Sn–8Zn–3Bi (Magnification 100 \times) aged at 150 °C for 100 h

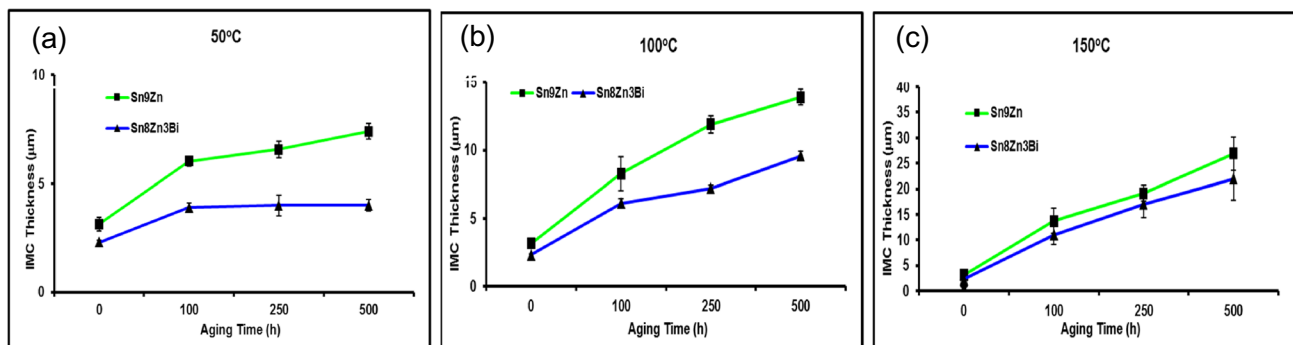
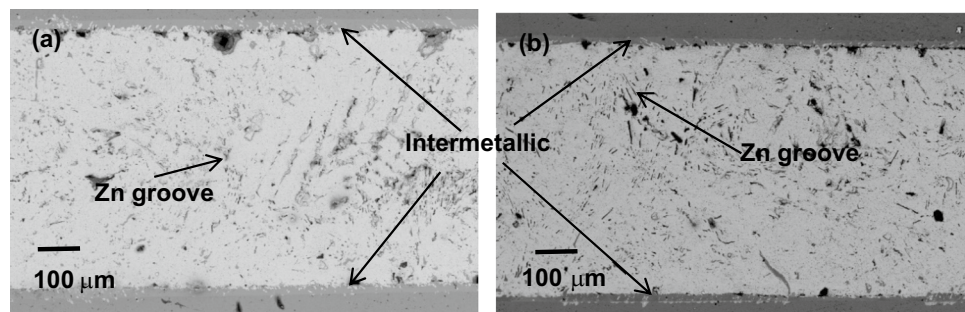


Fig. 10 Intermetallic thickness for Sn–9Zn/Cu and Sn–8Zn–3Bi/Cu joint aged until 500 h **a** 50 °C **b** 100 °C **c** 150 °C

either solder. However, the Sn–8Zn–3Bi solder had higher strain values than the Sn–9Zn solder. A smaller IMC layer thickness for the Sn–8Zn–3Bi/Cu joints contributed to the ductility of the joint.

Aging at 100 and 150 °C significantly degraded the solder joint strain at failure for the Sn–9Zn and Sn–8Zn–3Bi solders. For the Sn–9Zn solder, aging at 100 °C for 100 h reduced the strain at failure by 35% and further by 10 and 21% when the aging time was increased to 250 and 500 h, respectively. When the aging temperature was increased to 150 °C, after 100 h, the strain at failure degraded by 68% compared with the un-aged solder joint. After 250 h of aging, the failure strain decreased by 27%.

A similar trend was observed for the Sn–8Zn–3Bi solder joints. Aging at 100 °C for 100 h reduced the strain at failure by 34%, and further by 30 and 37% when the aging time continued to 250 and 500 h, respectively. When the aging temperature was increased to 150 °C, after 100 h, the strain at failure degraded by 73% compared with the un-aged solder joint. After 250 h of aging, the failure strain decreased by 36%. The increase in IMC thickness significantly reduced the ductility of the solder joints. However,

there was no significant difference in ductility between the Sn–9Zn and Sn–8Zn–3Bi solders when aging was performed at 100 and 150 °C.

Figure 12 shows the shear strength of the solder joints for Sn–9Zn and Sn–8Zn–3Bi solders. For as-soldered solder joint, Sn–8Zn–3Bi solder joint has higher shear strength of 25.1 MPa compared to Sn–9Zn which has 16.5 MPa. Thermal aging at 50 °C, the solder joint.

show no significant degradation for up to 500 h for both solders. The shear strength values remained at 15 MPa for Sn–9Zn and 23–28 MPa for Sn–8Zn–3Bi solder.

Although the shear strength did not degrade at aging temperature of 50 °C, the strength decreased as the aging temperature and time increased. At an aging temperature of 100 °C ($\sim 0.5T_m$) (T_m = melting temperature of solder) and aging time of 500 h, a significant reduction in the bonding strength was observed. Strength drops from 12.6 and 21.0 MPa to 10.5 and 11.3 MPa for Sn–9Zn and Sn–8Zn–3Bi solder joints, respectively. Further aging at 150 °C ($\sim 0.7T_m$) reduces shear strength significantly to 5.5 and 5.2 MPa for Sn–9Zn and Sn–8Zn–3Bi solder joints, respectively after 250 h of aging. Results on aging for 500 h could not be

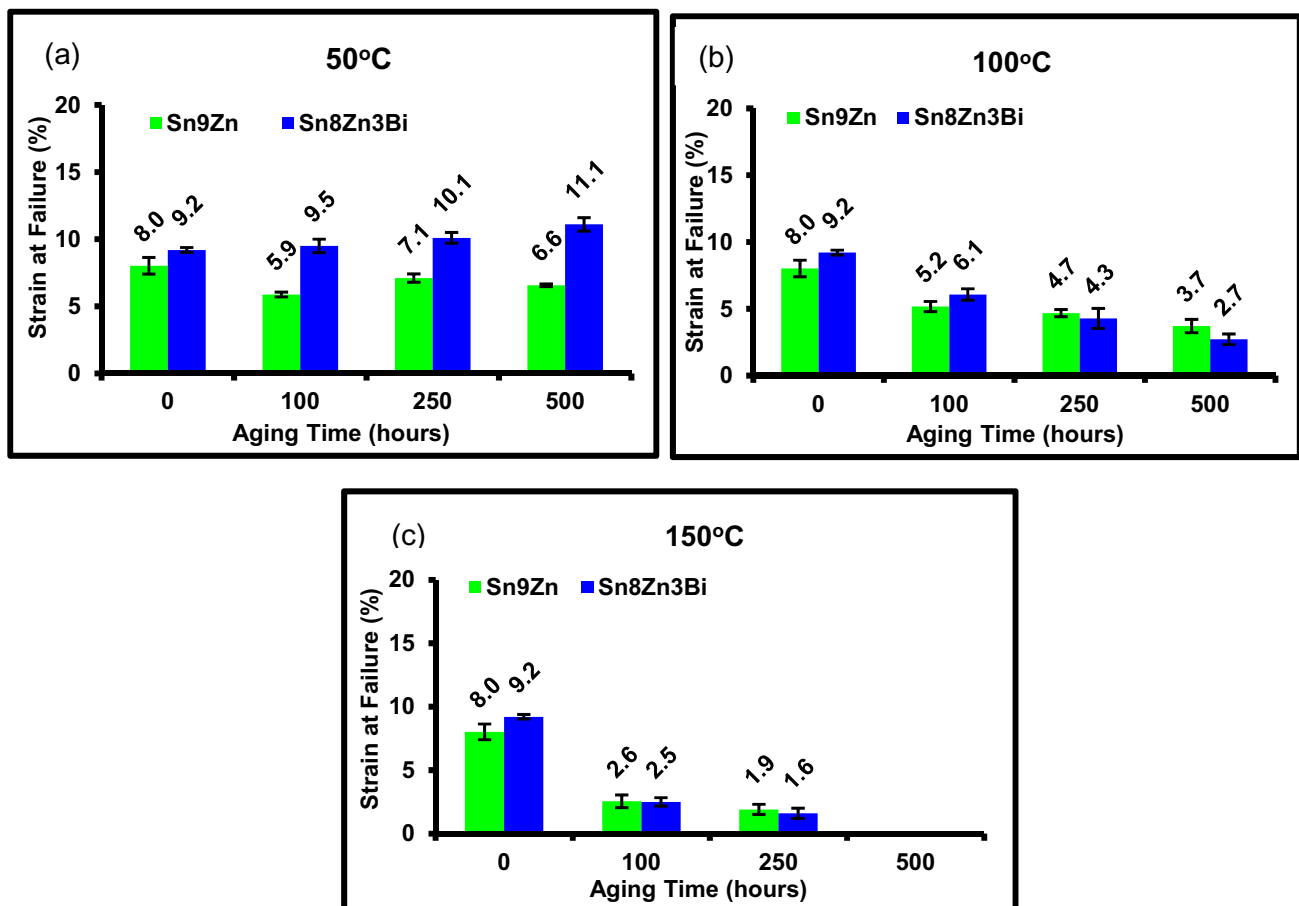


Fig. 11 Strain at failure for Sn–9Zn and Sn–8Zn–3Bi solder joints at different aging time a 50 °C b 100 °C c 150 °C

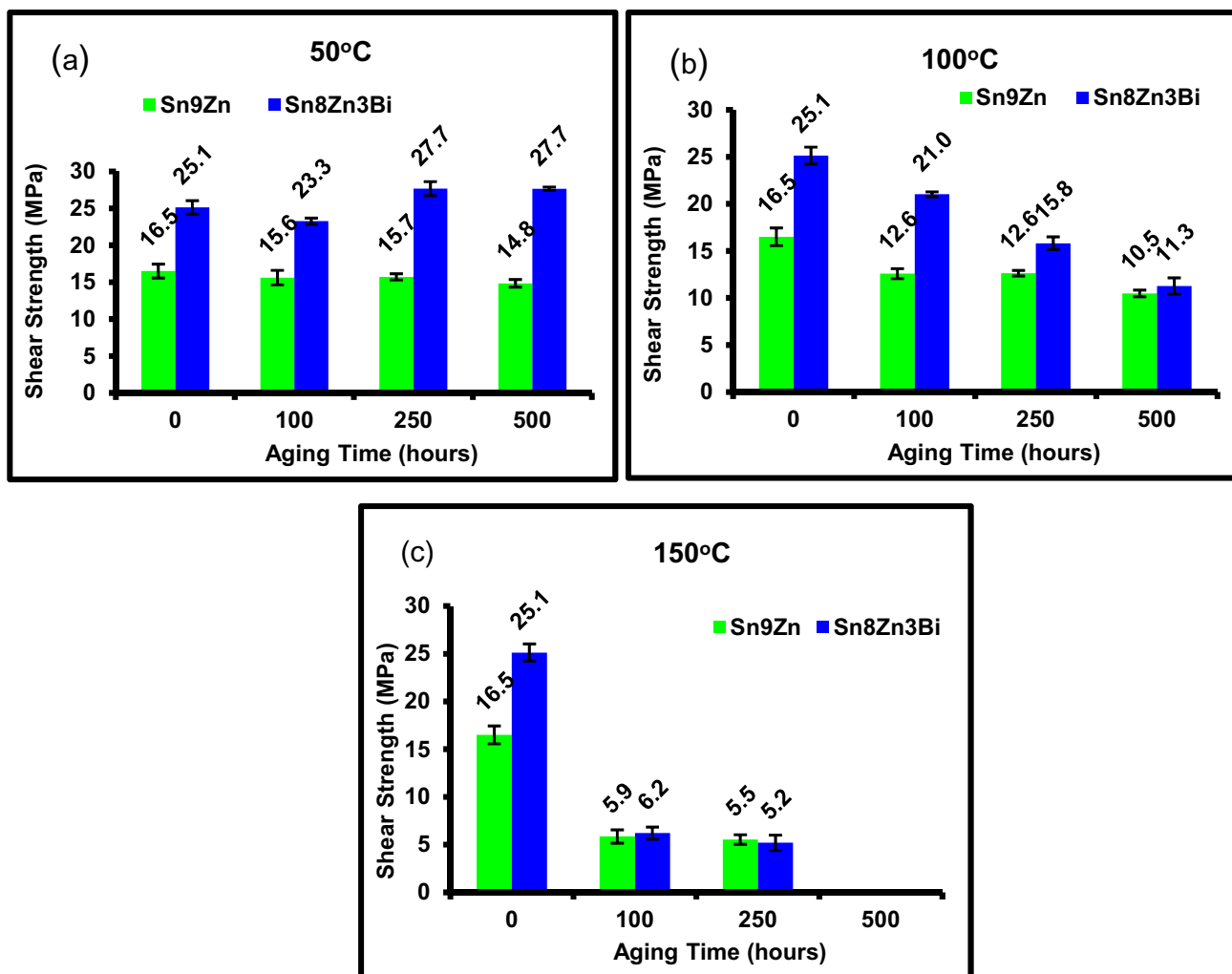


Fig. 12 Shear strength of Sn–9Zn and Sn–8Zn–3Bi solder joints a 50 °C b 100 °C c 150 °C

obtained because solder joints break even before they are clamped to the Instron machine.

In Sn–9Zn and Sn–8Zn–3Bi solders, the strength of the solder joint degrades after aging because of the thicker Cu_5Zn_8 intermetallic layer. As mentioned earlier, this brittle failure may be caused by cracks and/or stress in the intermetallic layer owing to differences in the thermal expansion coefficients.

After aging at 150 °C, the drop in the shear strength of these solder joints becomes more obvious. The back diffusion of Sn into the Cu side behind the reaction layer, forming a Sn-depletion zone, may have contributed to the decrease in the shear strength. Excessive growth of the Cu_5Zn_8 phase, which consumed Zn from the solder and generated a Zn-depletion zone near the interface, might also be another reason for solder degradation near the intermetallic/solder interface. Furthermore, the diffusion of Sn and Zn atoms near the intermetallic layer produced Kirkendall voids. These results contribute to

a reduction in the effective area to resist the tensile load and result in a reduced joint strength as reported by some researchers [13].

Solder joint failure is generally attributed to excessive growth of the intermetallic layer and formation of voids near the intermetallic/solder boundary. A very thick intermetallic layer may lead to structural defects owing to a mismatch in the coefficient of thermal expansion between the intermetallic and the substrate. Furthermore, excessive intermetallic growth might elevate internal defects, thereby reducing the solder joint strength. Hence, the growth of intermetallics and the formation of voids near the interface decrease the shear strength as aging progresses.

Fig. 13 As-soldered joint fracture path **a** Sn–9Zn/Cu **b** Sn–8Zn–3Bi/Cu

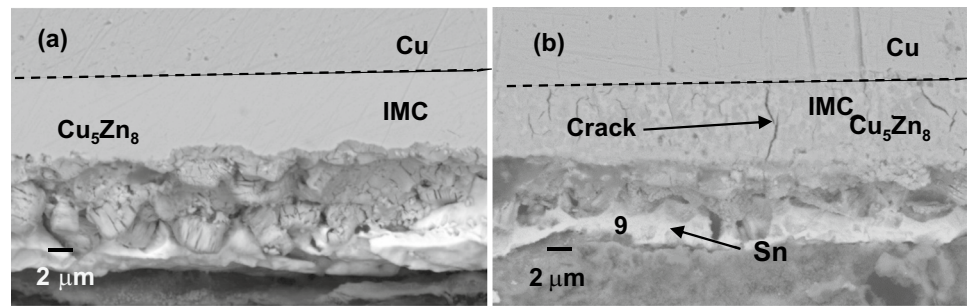


Fig. 14 Fracture path in **a** Sn–9Zn/Cu (150 °C, 500 h) and **b** Sn–8Zn–3Bi/Cu (150 °C, 250 h)

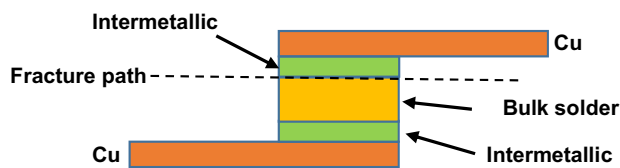
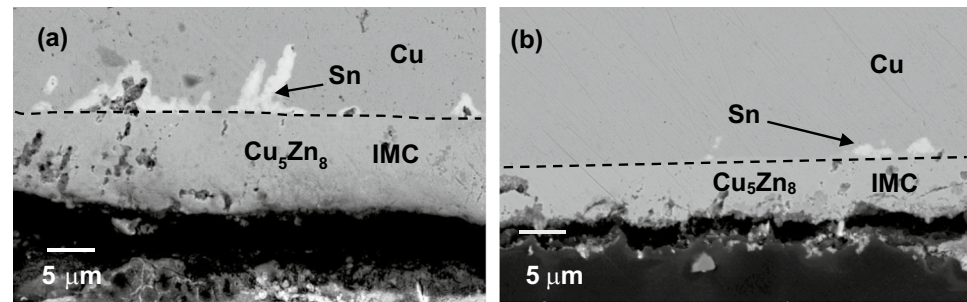


Fig. 15 Schematic diagram showing fracture path at intermetallic/solder boundary

3.3 Fracture Path and Surface Morphology in Solder Joint

FESEM was used to observe the fracture morphology in order to study the fracture behavior of the solder joints. Figures 13 and 14 show the fracture paths in the Sn–9Zn/Cu and Sn–8Zn–3Bi/Cu joints, respectively. Fracture occurred at the solder/ Cu_5Zn_8 interface for both Sn–9Zn and Sn–8Zn–3Bi joints, regardless of the intermetallic layer thickness or aging conditions. The presence of Sn (bulk solder) at the solder/ Cu_5Zn_8 interface was observed at spot 9.

Figure 15 shows the fracture path along the intermetallic/solder boundary. The fracture paths for the Sn–9Zn/Cu and Sn–8Zn–3Bi/Cu interfaces were initiated and propagated along the solder/ Cu_5Zn_8 boundary owing to the Sn and Zn depletion zone and Kirkendall void formation, as mentioned earlier. Stress concentration occurs near the solder/IMC interface owing to the difference in the thermal expansion coefficient between the solder, IMC, and substrate.

When an intermetallic interface other than Cu_5Zn_8 was formed, a different fracture mechanism was observed. Hu

et al. fabricated a Cu/SAC305/Cu joint after isothermal aging [8]. During the initial aging process, the fracture path was within the bulk solder. At longer aging conditions, the fracture mode changed to within the Cu_6Sn_5 intermetallic phase. However, as aging progressed and the volume fraction of the Cu_3Sn intermetallic increased, the fracture mode was along the $\text{Cu}_6\text{Sn}_5/\text{Cu}_3\text{Sn}$ boundary. Finally, as microcracks increase at the intermetallic/Cu boundary, the fracture changes to the $\text{Cu}_3\text{Sn}/\text{Cu}$ mode. Choudhury and Ladani tested Cu/Sn3.5Ag/Cu solder joints and reported similar results [4]. They reported that fracture occurs along the bulk solder in ductile mode when the volume fraction of solder is higher than that of IMC. However, when the joint had a higher IMC ($\text{Cu}_3\text{Sn} + \text{Cu}_6\text{Sn}_5$) volume fraction compared to the bulk solder, fracture occurred within the intermetallic phase.

Figure 16 shows the fracture morphologies of the Sn–9Zn and Sn–8Zn–3Bi solder joints under different aging conditions. The effect of high-temperature aging is well illustrated in the Sn–9Zn and Sn–8Zn–3Bi solder joints. Both the solders exhibited a dimple structure. These dimples show evidence of plastic deformation, and ductile fracture occurred as a shear load was applied to the solder joint in the early stages of aging. From the EDX analysis, the fracture surface was mainly composed of Sn and some Zn atoms, as shown in Fig. 16 (bulk solder side). The detailed composition is 86 wt% Sn and 9 wt% Zn which is Sn–9Zn solder (Fig. 16b). When EDX was performed on the bulk solder side (Fig. 16c) at 100 °C and 250 h of aging, the composition showed 46 wt% Sn and 45 wt% Zn. The reduction in the Sn content is attributed to the diffusion of Sn atoms towards the Cu

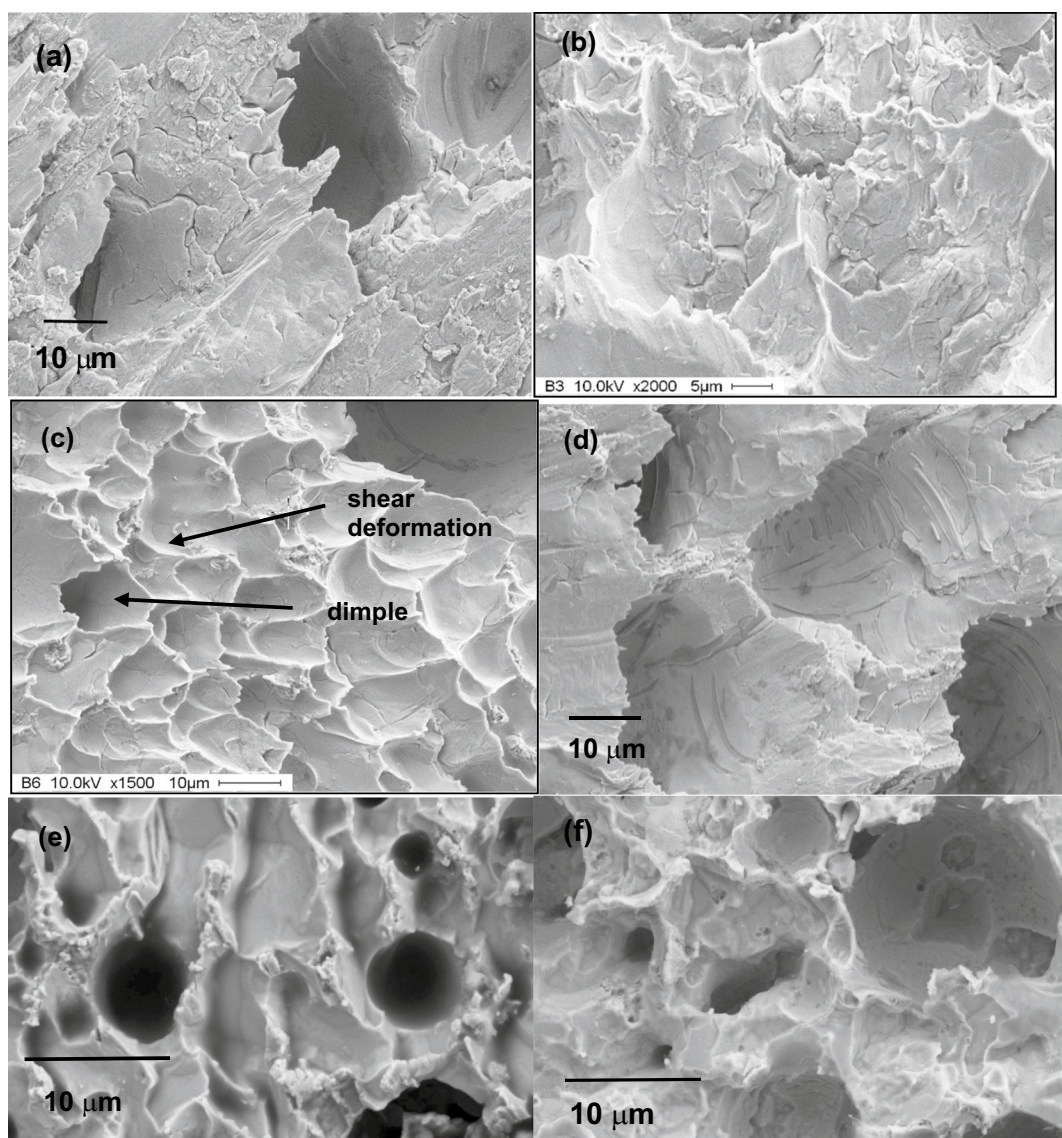


Fig. 16 FESEM micrograph Backscattered fracture surface taken at the bulk solder side for **a** Sn–9Zn joint as-soldered, **b** Sn–9Zn/Cu joint 50 °C, 250 h, **c** Sn–9Zn/Cu joint 100 °C, 250 h, **d** Sn–8Zn–

3Bi/Cu joint for as-soldered, **e** Sn–8Zn–3Bi/Cu joint 150 °C, 250 h, **f** Sn–8Zn–Bi solder joint 150 °C, 500 h

substrate at higher aging temperatures. These diffusions created a Sn-depletion zone along the intermetallic layer which weakened the solder joint. Therefore, shear fractures occur alongside the intermetallic layer and the bulk solder.

The fracture surfaces on the bulk solder side of the Sn–8Zn–3Bi solder are shown in Fig. 16d–f. The composition of the as-soldered joint (Fig. 16d) was, 86 wt% Sn and 9 wt% Zn and after 150 °C for 250 h aging, compositions were 73 wt% Sn and 11 wt% Zn. As mentioned before, the percentage of Sn decreased after aging, indicating the diffusion of Sn atoms near the boundary.

The fracture mode of the solder joint changed from ductile dimple failure to mixed brittle and dimple failure as

the aging time increased and total brittle failure at 500 h of aging. Therefore, aging at 50, 100, and 150 °C for 500 h causes the planar Cu_5Zn_8 phase to be the prevailing factor that prompt the fracture behavior.

4 Conclusions

This study investigated the interfacial intermetallic evolution and shear fracture behavior of Cu/Sn–9Zn/Cu and Cu/Sn–8Zn–3Bi/Cu solder joints after soldering and isothermal aging using a single lap-shear test. For all aging temperatures and times, only a single layer of Cu_5Zn_8 intermetallic

compound was observed. At a later stage, an isolated Cu_6Sn_5 intermetallic compound on the Cu side was observed. The presence of Bi retarded intermetallic growth in Sn–8Zn–3Bi/Cu–, and increased the joint strain and strength. Hence, the Sn–8Zn–3Bi/Cu joint was more ductile than the Sn–9Zn/Cu joint. The fracture mode displays ductile failure at lower aging temperatures and times-, but shows brittle failure at higher aging temperatures and longer times. For all aging temperatures and times, the failure mode occurred along the solder/intermetallic boundary resulting from the diffusion of Sn and Zn atoms, which weakened the boundary. Thus, Sn–9Zn/Cu and Sn–8Zn–3Bi/Cu joints at all aging temperatures and times experienced single fracture paths along the solder/IMC interface due to the formation of a single Cu_5Zn_8 intermetallic layer.

Acknowledgements This study was financially supported by the Ministry of Higher Education (MOHE) under Grant 600-RMI/FRGS 5/3 (104/2015). The author also thank the Universiti Teknologi MARA and Universiti Sains Malaysia for their facilities.

Author Contributions All authors contributed to this research. Material preparation, data collection, analysis and manuscript writing were performed Ramani Mayappan. Zainal Arifin Ahmad supervised the research and prove read the manuscript.

Funding This work was supported by Ministry of Higher Education (MOHE) under Grant 600-RMI/FRGS 5/3 (104/2015).

Research Data Policy and Data Availability Statements The authors declare that the data supporting the findings of this study are available within the paper.

Declarations

Conflict of interest The authors declare that they have no known competing financial interests or personal relationships that could have appeared to influence the work reported in this paper.

Human and Animal Rights Statement All procedures performed in studies do not involve human participants.

References

- J. Chen, H. Zhang, P. Zhang, Z. Yu, Y. Zhang, C. Yu, H. Lu, The Zn accumulation behavior, phase evolution and void formation in Sn-xZn/Cu systems by considering trace Zn: a combined experimental and theoretical study. *J. Market. Res.* **8**(5), 4141–4150 (2019)
- S. Cheng, C.-M. Huang, M. Pecht, A review of lead-free solders for electronics applications. *Microelectron. Reliab.* **75**, 77–95 (2017)
- S.F. Choudhury, L. Ladani, Effect of intermetallic compounds on the thermo-mechanical fatigue life of the three-dimensional integrated circuit package microsolder bumps: finite element analysis and study. *J. Electron. Packag.* **137**(4), 041003 (2015)
- S.F. Choudhury, L. Ladani, Local shear stress-strain response of Sn–3.5Ag/Cu solder joint with high fraction of intermetallic compounds: experimental analysis. *J. Alloy. Compd.* **680**, 665–676 (2016)
- M.N. Collins, J. Punch, R. Coyle, Surface finish effect on reliability of SAC 305 soldered chip resistors. *Solder. Surf. Mount Technol.* **24**(4), 240–248 (2012)
- C.M. Gourlay, B. Arfaei, Advances in electronic interconnection materials. *JOM* **71**(1), 131–132 (2019)
- S.-H. Hu, T.-C. Lin, C.-L. Kao, F.-Y. Huang, Y.-Y. Tsai, S.-C. Hsiao, J.-C. Kuo, Effects of bismuth additions on mechanical property and microstructure of SAC-Bi solder joint under current stressing. *Microelectron. Reliab.* **117**, 114041 (2021)
- X. Hu, T. Xu, L.M. Keer, Y. Li, X. Jiang, Microstructure evolution and shear fracture behavior of aged $\text{Sn}_3\text{Ag}_{0.5}\text{Cu}/\text{Cu}$ solder joints. *Mater. Sci. Eng. A* **673**, 167–177 (2016)
- S.H.A. Jaffery, M.F.M. Sabri, S. Rozali, S.W. Hasan, M.H. Mahdavi, D.A.S. Al-Zubiady, B.R. Ravuri, Oxidation and wetting characteristics of lead-free Sn-0.7Cu solder alloys with the addition of Fe and Bi. *Microelectron. Reliab.* **139**, 114802 (2022)
- Y.-H. Ko, J.-D. Lee, T. Yoon, C.-W. Lee, T.-S. Kim, Controlling interfacial reactions and intermetallic Compound growth at the interface of a lead-free solder joint with layer-by-layer transferred graphene. *ACS Appl. Mater. Interfaces* **8**(8), 5679–5686 (2016)
- H. Li, R. An, C. Wang, Z. Jiang, In situ quantitative study of microstructural evolution at the interface of $\text{Sn}_{3.0}\text{Ag}_{0.5}\text{Cu}/\text{Cu}$ solder joint during solid state aging. *J. Alloy. Compd.* **634**, 94–98 (2015)
- B. Liao, H. Wang, W. Xiao, Y. Cai, X. Guo, Recent advances in method of suppressing dendrite formation of tin-based solder alloys. *J. Mater. Sci. Mater. Electron.* **31**, 13001–13010 (2020)
- W. Liu, Y. Wang, Y. Ma, Q. Yu, Y. Huang, Interfacial microstructure evolution and shear behavior of Au–20Sn/(Sn)Cu solder joints bonded at 250 °C. *Mater. Sci. Eng. A* **651**, 626–635 (2016)
- L. Liu, P. Wu, W. Zhou, Effects of Cu on the interfacial reactions between Sn–8Zn–3Bi_xCu solders and Cu substrate. *Microelectron. Reliab.* **54**(1), 259–264 (2014)
- Y. Liu, F. Sun, Y. Liu, X. Li, Effect of Ni, Bi concentration on the microstructure and shear behavior of low-Ag SAC-Bi–Ni/Cu solder joints. *J. Mater. Sci. Mater. Electron.* **25**, 2627–2633 (2014)
- R. Mayappan, Z.A. Ahmad, Effect of Bi on the activation energy for the growth of Cu_5Zn_8 intermetallic in the Sn–Zn lead-free solder. *Intermetallics* **18**(4), 730–735 (2010)
- R. Mayappan, A.B. Ismail, Z.A. Ahmad, T. Ariga, L.B. Hussain, The effect of crosshead speed on the joint strength between Sn–Zn–Bi lead-free solders and Cu substrate. *J. Alloy. Compd.* **436**(1–2), 112–117 (2007)
- R. Mayappan, A.B. Ismail, Z.A. Ahmad, T. Ariga, L.B. Hussain, Effect of sample perimeter and temperature on Sn–Zn based lead-free solders. *Mater. Lett.* **60**(19), 2383–2389 (2006)
- Y. Mutoh, J. Zhao, Y. Miyashita, C. Kanchanomai, Fatigue crack growth behaviour of lead-containing and lead-free solders. *Solder. Surf. Mount Technol.* **14**(3), 37–45 (2002)
- H. Nishikawa, Y. Hirata, C.-H. Yang, S.-K. Lin, Effect of low Bi content on reliability of Sn-Bi Alloy joints before and after thermal aging. *JOM* **74**(4), 1751–1759 (2022)
- R. Pandher, R. Healey, Reliability of Pb-free solder alloys in demanding BGA and CSP applications, in *58th Electronic Components and Technology Conference IEEE*, New York, (2008), pp. 2018–2023
- G. Ren, M.N. Collins, On the mechanism of Sn tunnelling induced intermetallic formation between Sn–8Zn–3Bi solder alloys and Cu substrates. *J. Alloy. Compd.* **791**, 559–566 (2019)
- J. Shen, Y. Pu, D. Wu, Q. Tang, M. Zhao, Effects of minor Bi, Ni on the wetting properties, microstructures, and shear properties of Sn–0.7Cu lead-free solder joints. *J. Mater. Sci. Mater. Electron.* **26**, 1572–1580 (2015)

24. K. Sukanuma, K. Niihara, T. Shoutoku, Y. Nakamura, Wetting and interface microstructure between Sn–Zn binary alloys and Cu. *J. Mater. Res.* **13**(10), 2859–2865 (1998)
25. W. Wang, Z. Chen, S. Wang, X. Long, Mechanics-based acceleration for estimating thermal fatigue life of electronic packaging structure. *Microelectron. Reliab.* **107**, 113616 (2020)
26. M.-Y. Xiong, L. Zhang, Interface reaction and intermetallic compound growth behavior of Sn–Ag–Cu lead-free solder joints on different substrates in electronic packaging. *J. Mater. Sci.* **54**(2), 1741–1768 (2019)
27. S. Zhang, X. Xu, T. Lin, P. He, Recent advances in nano-materials for packaging of electronic devices. *J. Mater. Sci. Mater. Electron.* **30**(15), 13855–13868 (2019)
28. J. Zhao, Y. Mutoh, Y. Miyashita, S.L. Mannan, Fatigue crack-growth behavior of Sn–Ag–Cu and Sn–Ag–Cu–Bi lead-free solders. *J. Electron. Mater.* **31**, 879–886 (2002)
29. J. Zhao, C.Q. Cheng, L. Qi, C.Y. Chi, Kinetics of intermetallic compound layers and shear strength in Bi-bearing SnAgCu/Cu soldering couples. *J. Alloy. Compd.* **473**, 382–388 (2009)
30. J. Zhao, L. Qi, X.M. Wang, L. Wang, Influence of Bi on microstructures evolution and mechanical properties in Sn–Ag–Cu lead-free solder. *J. Alloy. Compd.* **375**(1–2), 196–201 (2004)

Publisher's Note Springer Nature remains neutral with regard to jurisdictional claims in published maps and institutional affiliations.

Springer Nature or its licensor (e.g. a society or other partner) holds exclusive rights to this article under a publishing agreement with the author(s) or other rightsholder(s); author self-archiving of the accepted manuscript version of this article is solely governed by the terms of such publishing agreement and applicable law.